

Investigations on the structural and optical properties of RF magnetron sputtered TiO₂ thin films: effect of substrate temperature and Ar:O₂ ratio

PRABITHA B. NAIR, V. B. JUSTINVICTOR, GEORGI P. DANIEL, K. JOY, K. C. JAMES RAJU^a, P. V. THOMAS*
*Thin Film Lab, Post Graduate and Research Department of Physics, Mar Ivanios College,
Thiruvananthapuram 695015, Kerala, India*
^a*School of Physics, University of Hyderabad, Central University P. O., Hyderabad 500046, India*

TiO₂ thin films were deposited onto quartz substrates by RF magnetron sputtering at different substrate temperature and Ar:O₂ ratios using TiO₂ ceramic target and then annealed at 873 K for 2 h. The films deposited at low substrate temperature (ST) were amorphous-like but possessed short range order as shown by the Raman shifts. In films prepared by sputtering technique, we have found that better crystallinity to anatase phase is possible by thermal annealing only if films are deposited at suitable substrate temperature. Though band gap was found to increase with both substrate temperature and Ar:O₂ ratios, better tunability of band gap from 3.61-3.78 eV was achieved by increasing the Ar:O₂ ratio. The increase in optical band gap from that of the bulk in both cases is attributed to quantum confinement effect. Refractive index decreased when substrate temperature was increased upto 473 K after which it showed an increase. Increase of oxygen content resulted in the decrease of refractive index from 2.56 to 2.38, which is attributed to the variation of the packing density. It was observed that substrate temperature and Ar:O₂ ratio strongly affected the PL spectra of the films.

(Received October 18, 2012; accepted March 13, 2014)

Keywords: TiO₂ thin films, RF magnetron sputtering, Micro Raman analysis, AFM, Optical constants, Photoluminescence

1. Introduction

Titanium dioxide (TiO₂) is a technologically important material widely used in optical and electronic applications. Ever since the discovery of photo-induced water cleavage on TiO₂ electrodes by Fujishima and Honda in the early 1970s [1] the material has attracted significant attention. When exposed to ultraviolet light, holes (h_{VB}^+) and excited electrons (e_{CB}^-) are generated. The hole is capable of oxidising water or hydroxide anions to hydroxyl radicals (.OH). [2, 3]. .OH is a powerful oxidizing agent to degrade a wide range of organic pollutants, such as aromatics and aliphatics, dyes, pesticides and herbicides [4, 5, 6]. Other numerous technological applications of TiO₂ coatings include its prospective use as a material for smart windows [7], antireflective coatings [8] optical filters [9], solar energy conversion systems [10,11], protective layers for very large scale integrated circuits [12], gas sensors[13] and electro chromic materials for display devices [10,14]. Dye sensitized solar cells based on TiO₂ has attracted wide attention since the reports on their fabrication by Regan and Gratzel [15] because of low cost of the material, long term stability against photo-corrosion and chemical corrosion, and eco - friendly photovoltaic ability with good efficiency comparable to those of silicon cells.

TiO₂ exists in amorphous form and in three crystalline forms: anatase (A), rutile (R) and brookite (B). The amorphous state is used for optical coatings because of its optical anisotropy. Also due to its unique blood compatibility, amorphous titania films are promising

candidates in biomedical field. TiO₂ in anatase phase are usually n type semiconductors due to point defects in their crystalline structure [16]. Anatase phase is used in dye - sensitized solar cells due to its higher band gap. Anatase is also highly preferred for its pronounced photocatalytic activity and for its wetting behaviour which results in antifogging effect [17, 18]. Rutile TiO₂ is widely used for dielectric layers due to its high dielectric constant and in antireflective coatings due to its higher refractive index. [17, 18, 19]. Anatase is a low temperature metastable phase and rutile is the most stable of the three phases. The crystal structure of TiO₂ can be described as two chains of differently distorted TiO₆ octahedra. TiO₆ octahedra are interconnected differently for each phase, leading to different structures and symmetries. Anatase TiO₂ is tetragonal with lattice parameters $a = 0.378$ nm, $c = 0.9514$ nm, and refractive index of 2.54. Rutile is tetragonal with lattice parameters $a = 0.4594$ nm, $c = 0.2958$ nm and refractive index of 2.7. Brookite phase is orthorhombic with lattice parameters, $a = 0.9184$ nm, $b = 0.5447$ nm, $c = 0.5145$ nm [20]. The differences in assembly patterns within the chains and in the lattice structures result in different band structure and band gap of the two phases: 3.20 eV for anatase and 3.02 eV for rutile [21].

TiO₂ thin films can be prepared by a variety of methods such as thermal [22] or anodic [23] oxidation of titanium, electron beam evaporation [24], RF magnetron sputtering [25, 26], chemical vapor deposition [11, 27], including plasma-enhanced chemical vapor deposition [28], sol-gel method [29] and pulsed laser deposition [30]. Of these methods, RF magnetron sputtering has proved to

be a promising technique for depositing large scale, highly dense and uniform TiO₂ thin films, which have strong adherence to the substrates. Though the material has been widely investigated over the years, there are varied reports in literature regarding the crystallinity, optical band gap and the associated optical constants viz., refractive index, extinction coefficient etc., of TiO₂ films prepared by sputtering technique. Mostly TiO₂ films deposited by classical magnetrons are amorphous or not well crystalline. One way to prepare crystalline TiO₂ films directly is by the application of pulsed magnetron discharges [16]. Post deposition thermal annealing is another method to obtain crystalline coatings. Thermally annealed, RF magnetron sputtered TiO₂ thin films are crystalline in nature as reported by Q. Ye et al, M. M. Hasan et al and N. Martin et al [31, 32, 33]. But RF magnetron sputtered films exhibited only a very weak crystallinity to anatase phase as reported by D. Yoo et al and S. Dangtip et al [34, 35]. Though crystalline TiO₂ thin films were deposited by DC magnetron sputtering by L. Baoshun et al, the extent of crystallinity was low in these films [36]. The reported optical properties also show variations. Hence investigations on the dependence of crystallinity and optical constants of the RF sputtered TiO₂ thin films on the deposition parameters are of importance.

The sputtering conditions such as working pressure, Ar:O₂ ratio, RF power, substrate temperature and post-deposition annealing techniques can be controlled and optimized to obtain high quality thin films with well defined microstructure suitable for a variety of applications. We have earlier reported the effect of RF power and sputtering pressure on the structural, optical and photoluminescence properties of RF magnetron sputtered TiO₂ thin films [37]. In this work, the effect of substrate temperature and Ar:O₂ ratio on the structural, optical and PL properties of TiO₂ thin films prepared by RF magnetron sputtering has been investigated. We have observed that precise control of optical properties can be achieved by varying the above parameters which enables the use of these films for device applications.

2. Experimental details

TiO₂ thin films were deposited onto quartz substrates by RF magnetron sputtering of a ceramic TiO₂ (99.99%, Sigma-Aldrich) target. Amorphous quartz substrates were chosen for film deposition as they are transparent, strong, electrically insulating and inert. Prior to deposition the substrates were cleaned ultrasonically in acetone, rinsed in deionized water and dried in nitrogen gas flow. The target was prepared by a standard procedure as reported in our previous paper [37]. The target-substrate distance was 5 cm. Sputtering was carried out for 3 h at RF power of 300 W. All the films were post - annealed in air for 2 h in a muffle furnace at 873 K. In order to investigate the effect of substrate temperature on the structural and optical properties of TiO₂ thin films, substrate temperature was varied as 300, 473, 523 and 573 K. The samples obtained were coded ST1, ST2, ST3 and ST4, respectively. The working gas, high purity argon, was maintained at a

pressure of 0.01 mbar. To analyze the effect of Ar:O₂ ratio on the structural and optical properties of TiO₂ thin films, the Ar:O₂ ratio was varied as 100:0, 70:30 and 50:50. The samples were coded AO1, AO2 and AO3, respectively. The sputtering pressure was kept at 0.015 mbar.

The structure of the films was examined by using X-ray diffraction technique with Cu K α radiation ($\lambda=0.154$ nm) in a Bruker AXS D8 Advance standard X-ray diffractometer. Micro Raman analysis of the samples was done using a Labram-HR 800 spectrometer equipped with an argon ion laser. SEM images and EDX were recorded using Jeol Model JSM-6390LV microscope. AFM images were recorded using a SPA-400, SII, Inc. Japan atomic force microscope operated in non contact mode. UV-vis transmission spectra were recorded with a JASCO V-550 spectrophotometer in the wavelength range: 300 - 900 nm. Film thickness (t), refractive index (n) and extinction coefficient (k) were calculated by Swanepoel's envelope method [38]. Photoluminescence spectra of the films were recorded by a Perkin Elmer LS 55 spectrofluorometer, equipped with a 40W Xenon lamp, and excited at 320 nm.

3. Results and discussion

3.1 X-ray diffraction studies

Fig. 1 shows the X-ray diffraction patterns of TiO₂ thin films deposited at various substrate temperatures and post - annealed at 873 K. Films deposited at room temperature (ST1) exhibited a mixed phase (A+R). Weak peaks corresponding to A(002) and R(101) planes were observed at $2\theta = 18.5706$ and 36.2870° respectively. The film ST2, deposited at 473 K exhibited an amorphous structure. The films deposited at higher substrate temperatures of 523 and 573 K (ST3 and ST4) exhibited pure anatase structure. Weak diffraction peak from A(002) plane was observed at $2\theta = 18.5706^\circ$ for the film ST3. Diffraction peaks of significant intensity corresponding to A(101), A(004) and A(200) planes were observed at $2\theta = 25.3862$, 37.8098 and 48.1960° , respectively for the film ST4. With increase in substrate temperature, the surface mobility of the deposited atoms increases and they diffuse to equilibrium sites, thereby increasing the crystallinity. Post-deposition thermal annealing also favors this phenomenon. Hence the film ST4 shows better crystallinity compared to the films deposited at lower substrate temperatures.

Fig. 2 shows the XRD patterns of TiO₂ films deposited at various Ar:O₂ ratios and post annealed at 873 K. No diffraction peak is observed in these samples, which suggest an amorphous structure of the films. For crystallization to occur in thin films, the deposited atoms should have sufficient energy for surface diffusion. Here, since the substrates are maintained at room temperature, the formation of amorphous phase in TiO₂ thin films can be attributed to low surface mobility of deposited atoms. Also, since the total pressure was maintained at 0.015 mbar, when oxygen content is increased, the amount of argon ions available for sputtering decreases, which results in lowering of sputtering yield. Moreover increase in

oxygen content causes scattering of sputtered species, resulting in the formation of amorphous films.

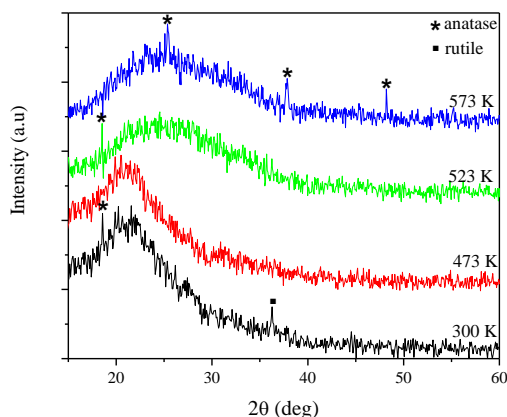


Fig. 1. XRD patterns of TiO_2 thin films deposited at various substrate temperatures (300 W, 0.01 mbar) and post annealed at 873 K.

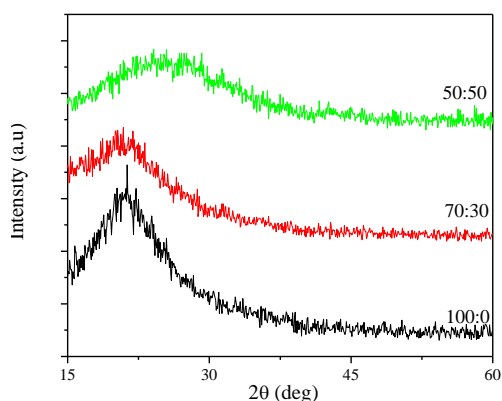


Fig. 2. XRD patterns of TiO_2 thin films deposited at various Ar: O_2 ratios (300 W, 0.015 mbar) and post annealed at 873 K.

Though the films deposited in the temperature range 300-523 K are amorphous – like in nature, it should be noted that these amorphous-like XRD patterns just denote the absence of long range order in these films. This absence of long range order and presence of short range order in RF magnetron sputtered TiO_2 thin films have been confirmed in our earlier studies [37]. It has also been reported by M. Sreemany *et al* that amorphous-like TiO_2 films consists of nanostructured crystalline networks with extremely small sizes, which are below the detection limit of X-rays [39]. Since the films under consideration (except the film ST4) are amorphous-like in nature, the detection limit of XRD does not allow unambiguous identification of phases. Hence micro Raman spectra were recorded to identify the phase composition in the samples.

3.2 Micro Raman analysis

Anatase TiO_2 exhibits D_{4h}^{19} - $I4_1/amd$ symmetry whereas rutile TiO_2 exhibits D_{4h}^{14} - $P4_2/mnm$ symmetry. 15 optical modes with irreducible representations, $1A_{1g} + 1A_{2u} + 1B_{1g} + 1B_{2u} + 3E_g + 2E_u$ has been identified for anatase TiO_2 by factor group analysis, of which only A_{1g} ,

B_{1g} and E_g are Raman active [40]. The shape and position of Raman bands depend mainly on the crystallization, stress/strain, structural disorder/defects and the presence of dopants. According to the molecular theory of vibrations, these factors will lead to neighboring disorder and local geometric disorientation, affecting the Raman bending and stretching mode vibrations. The observed band positions in our experiment agree well with the reported values [41, 42, 43].

Fig. 3 shows the micro Raman vibrational spectra for the films deposited at various substrate temperatures. Raman active modes at 141.79, 196.95, 395.53, 516.5 and 636.23 cm^{-1} corresponding to anatase phase and at 445.67 and 607.81 cm^{-1} corresponding to rutile phase were observed in the film ST1. Raman active modes was observed at 142.46, 393.52, 489.67 cm^{-1} (anatase) and 811.07 cm^{-1} (rutile) for the film ST2. Thus micro Raman spectrum indicates the formation of mixed phase (A+R) in the films deposited at lower substrate temperature. Though the film ST2 was XRD-amorphous, micro Raman analysis confirmed the presence of anatase and rutile phases in this film. Raman active modes corresponding to anatase phase was observed at 143.12, 394.86, 493.81 cm^{-1} and at 143.12, 198.62, 396.53, 518.55, 636.56 cm^{-1} for the films ST3 and ST4 respectively. XRD analysis also indicated pure anatase structure for these films.

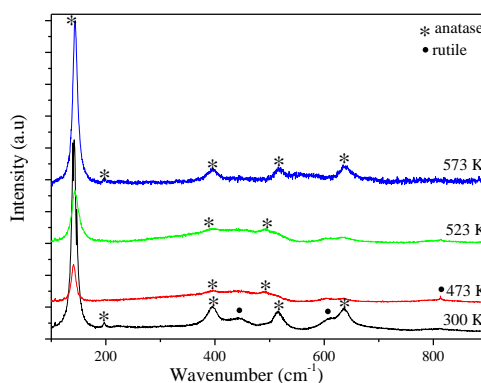


Fig. 3. Micro Raman spectra of TiO_2 thin films deposited at various substrate temperatures (300 W, 0.01 mbar) and post annealed at 873 K.

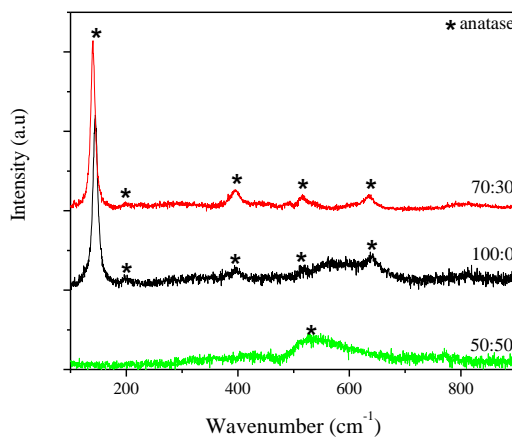


Fig. 4. Micro Raman spectra of TiO_2 thin films deposited at various Ar: O_2 ratios (300 W, 0.01 mbar) and post annealed at 873 K.

Fig. 4 shows the micro Raman spectra for the films AO1, AO2 and AO3, deposited at various Ar:O₂ ratios. Raman active modes of vibration corresponding to the anatase phase was observed at 143.87, 197.83, 395.72, 515.03, 639.92 cm⁻¹ and at 140.14, 199.69, 395.73, 516.89, 634.14 cm⁻¹ for the films AO1 and AO2, respectively. Intensity of the main peak at 144 cm⁻¹ increased for the film deposited at the Ar:O₂ ratio 70:30 (AO2), which denotes better structural order and crystallinity of the film. But the film deposited in the Ar:O₂ ratio 50:50 (AO3) exhibited only a weak and broad Raman band at 532.39 cm⁻¹. This is due to increase in amorphous nature of the films as a result of lower sputtering yield. Optimal Ar:O₂ ratio for obtaining better films is 70:30. It may be noted that all the samples except AO3 suffer from tensile stress, which is indicated by the shift in the position of Raman bands towards lower wave numbers [44].

Combining the XRD and micro Raman analysis it may be concluded that lower substrate temperature favors faster transformation to rutile phase on annealing, whereas the films deposited at higher substrate temperature resulted in better crystallization to anatase phase. As oxygen

content in the sputtering chamber is increased (70:30), the films showed better crystallization to anatase phase, whereas, at higher oxygen content (50:50), the films are amorphous in nature.

3.3 Surface studies

SEM images and energy dispersive X-ray (EDX) spectrum of the samples deposited at different substrate temperatures and that of sample prepared in the Ar:O₂ ratio 70:30 (AO2) are shown in Fig. 5. All the films present a continuous and crack free surface. According to Thornton's structure zone model, a porous film structure is formed owing to low atom mobility under low substrate temperature [45]. The porous nature of the film ST1 is evident in the SEM images. EDX spectrum shows only two prominent peaks, corresponding to titanium and oxygen. This indicates the purity of the deposited films and that no other elements other than Ti and O are present in the samples. But a quantitative analysis of the formation of TiO₂ is difficult as the oxygen *K* α line will have contribution from the quartz substrate also.

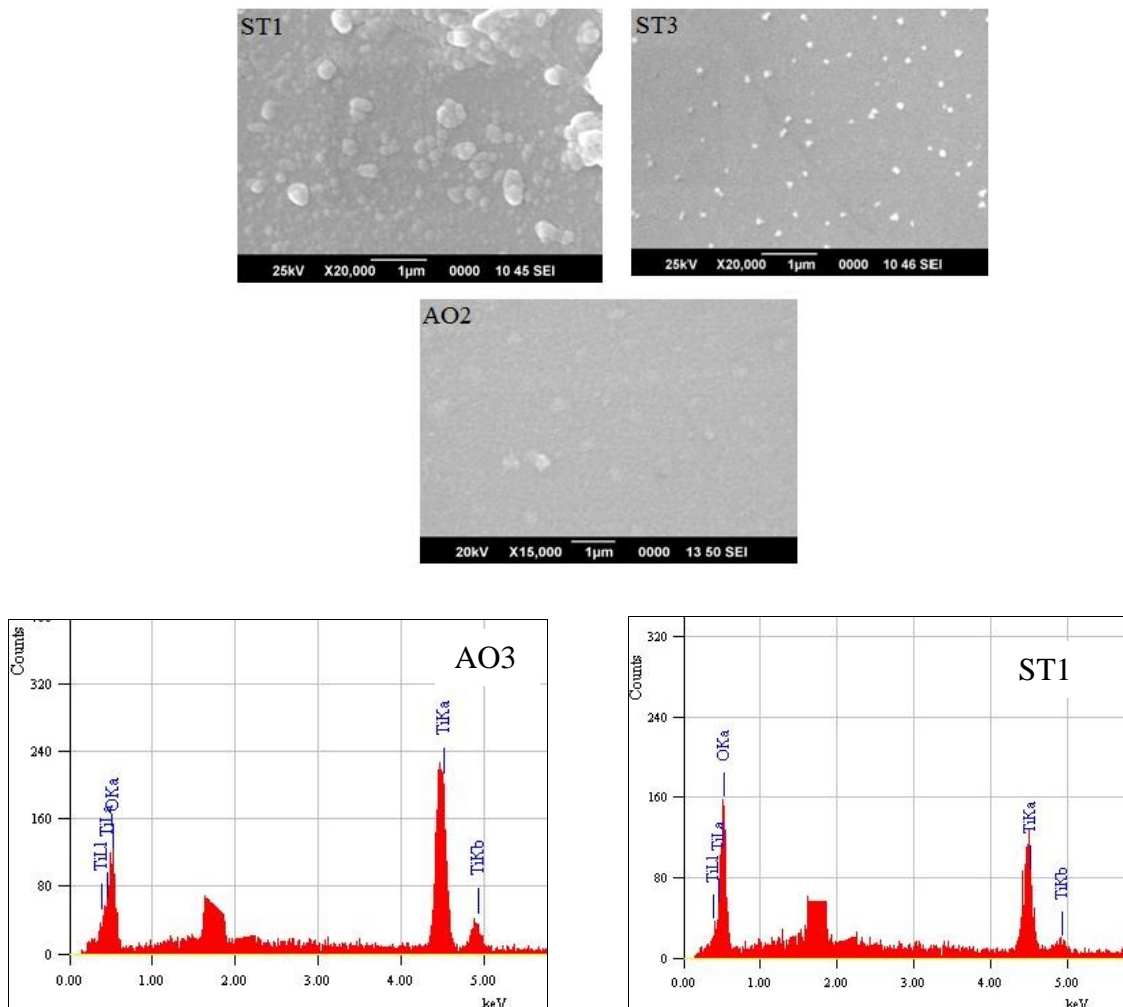


Fig. 5. SEM images and EDX spectrum of TiO₂ thin films deposited on quartz substrates and post annealed at 873 K.

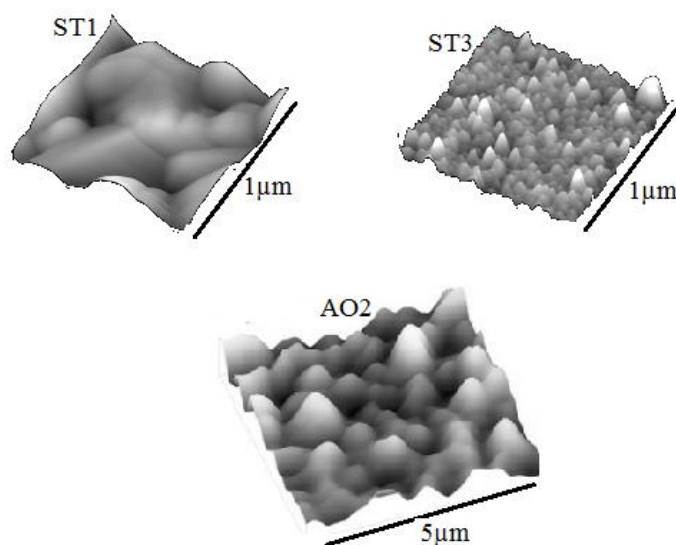


Fig. 6. AFM images of TiO_2 thin films deposited on quartz substrates and post annealed at 873 K.

AFM images of the same samples are shown in Fig. 6. All the films present a rough surface texture consisting of particles fused together at the inter particle contact, building up high mountains and deep valleys. Surface roughness was found to decrease with increase in substrate temperature. The roughness values are 3.36 and 2.10 for the samples ST1 and ST3, respectively. Roughness value was higher for the samples sputtered in $\text{Ar}:\text{O}_2$ atmosphere (24.579 for the sample AO2). T. Takahashi has earlier reported that surface roughness is higher for films deposited at larger oxygen pressures [46]

3.4 Optical studies

UV-visible spectroscopy was used to calculate the optical band gap and optical constants of the samples. Figs. 7 and 8 shows the optical transmittance as a function of wavelength for TiO_2 thin films deposited at various substrate temperatures and various $\text{Ar}:\text{O}_2$ ratios, respectively. The band fluctuations observed in the spectra is due to the optical interference in films due to the difference in refractive index of the film and substrate and increases with film thickness. Films are transparent in the visible region and a sharp fall in transmittance is observed in the UV region, which corresponds to the absorption edge. This fall below 360 nm is due to the excitation of electrons from the valence band to the conduction band of TiO_2 . In TiO_2 the Ti-derived 3d bands are unoccupied and split into t_{2g} and e_g sub-bands by the octahedral crystal field. The energy band structure of TiO_2 in the band gap region consists of O 2p states in the valence band and Ti 3d states with t_{2g} character in the conduction band. Thus, the optical band-gap edge of TiO_2 is assigned to direct interband transitions from the valence-band edge with O 2p character to the conduction band edge with Ti 3d (t_{2g}) character [47].

The thickness of the samples was calculated using Swanepoel's envelope method. Thickness of the films

prepared at room temperature was found to be greater than that of films prepared at higher substrate temperatures. Optical band gap E_g was calculated using the Tauc equation [48]

$$\alpha h\nu = A(h\nu - E_g)^m \quad (1)$$

where A is a constant, $h\nu$, the photon energy (eV) and α , the absorption coefficient, determined using the relation

$$\alpha = t^{-1} \ln(1/T) \quad (2)$$

where t is the film thickness. The value of m can be 1/2 or 2 depending on whether the transitions are direct or indirect. The values of film thickness, direct optical band gap and other optical parameters are given in Table 1.

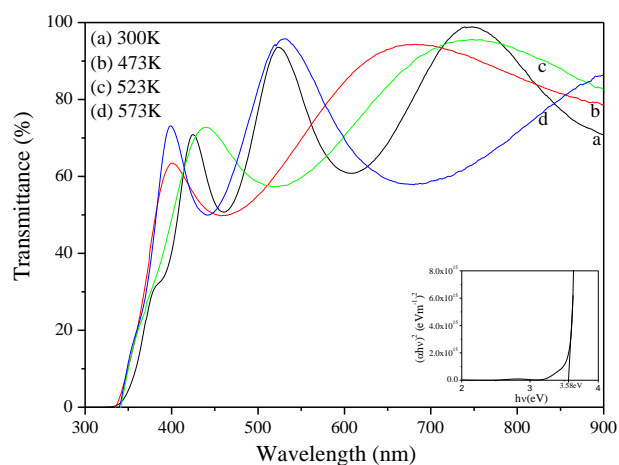


Fig. 7. UV-vis transmittance spectra of TiO_2 thin films deposited at various substrate temperatures (300 W, 0.01 mbar) and post annealed at 873 K. Inset shows the Tauc plot for the film deposited at room temperature.

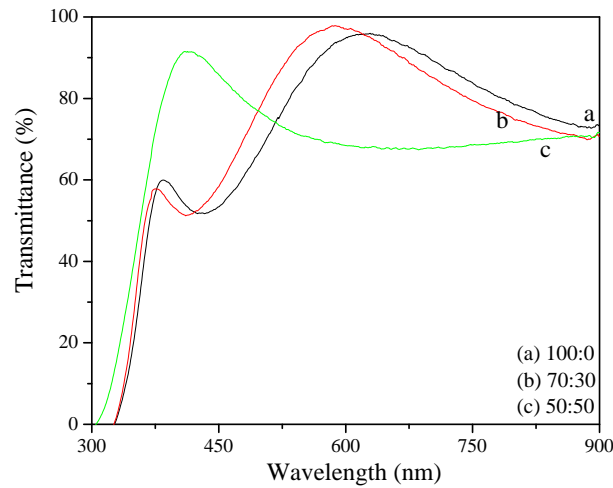


Fig. 8. UV-vis transmittance spectra of TiO₂ thin films deposited at various Ar-O₂ ratios (300 W, 0.015 mbar) and post annealed at 873 K.

Table 1. Variation of optical parameters and particle size with substrate temperature (ST1-ST4) and Ar:O₂ ratio (AO1-AO3).

Sample	Optical band gap (eV)	Thickness (nm)	Refractive index	Extinction coefficient	Particle size (nm)
ST1	3.58	290	2.79	0.0544	11.41
ST2	3.66	136	2.64	0.1246	10.37
ST3	3.65	191	2.65	0.1060	10.48
ST4	3.67	195	2.69	0.0740	10.26
AO1	3.61	225	2.56	0.0708	10.98
AO2	3.71	225	2.45	0.0694	9.85
AO3	3.78	180	2.38	0.0527	9.23

It is observed that, direct optical band gap increased from 3.58 to 3.66 eV with increase in substrate temperature from room temperature to 473 K. In nanostructured films, charges are localized in individual nanocrystals resulting in an increase in band gap [49]. Since the microstructural changes in a thin film material depend on the kinetics of growth and the substrate temperature, the uncompleted microstructures may be modified by giving thermal energy by post-deposition annealing treatment [50]. Decrease in disorder or defects in structural bonding resulting from post-deposition annealing also contribute to increase in optical band gap.

Direct optical band gap increases from 3.61 to 3.78 eV with increase in O₂ content in the chamber during sputtering. Similar observation has been reported by Asanuma et al for TiO₂ thin films deposited by reactive magnetron sputtering [51]. The increase in band gap can be attributed to reduction of oxygen vacancies in the film due to incorporation of more oxygen into the chamber [52]. Thus band gap tuning can be achieved by varying the Ar:O₂ ratio. The reduction in oxygen vacancies also leads to the absence of defect related photoluminescence emissions in sample AO2 as discussed later in section 3.5.

The blue shift of absorption edge observed in the transmittance spectra signifies a decrease in particle size with increase in O₂ content.

Optical band gap values of the prepared TiO₂ thin films are higher than that of the bulk. The larger band gap is due to the nanocrystalline nature of the films [41] and can be explained in terms of quantum size effect that emerges in semiconductors with small particle sizes in the range 1-10 nm [53]. Z. Lide et al has attributed the significant blue shift of the absorption edge compared to that of solid anatase (360 nm) as the consequence of exciton confinement with decrease in particle size (quantum effect of nanophase TiO₂) [54]. The electron and hole produced in quantum size particles are confined in a potential well of small geometrical dimensions. These electrons and holes do not experience the electronic delocalization present in bulk semiconductors which possesses a conduction and valance band. Instead, the confinement produces a quantization of discrete electronic states and increases the effective band gap of the semiconductor. Such effects can also change the colour of the material due to the different absorption maxima and also the photocatalytic properties of the films. The

expression for confinement energy can be used to calculate the particle size of the samples [37]. The values of particle size for the films prepared under various substrate temperatures and Ar:O₂ ratios is given in Table 1.

With increase in substrate temperature, surface mobility of the sputtered particles increases. This should result in the formation of a compact film. In our study, a decrease in refractive index (calculated at $\lambda=550$ nm) was observed with increase in substrate temperature from 300 to 473 K. This may be due to the decrease in thickness observed in the films deposited at 473 K. With further increase in substrate temperature, the diffusive ability of atoms or molecules increases which results in an increase in refractive index [55]. Also, the increase in refractive index with substrate temperature may be attributed to the increase in packing density and crystallinity of the films [56]. Extinction coefficient, evaluated using the equation [38]

$$k = \frac{\alpha\lambda}{4\pi} \quad (3)$$

at $\lambda=550$ nm, increased with increase in substrate temperature from 300 to 473 K, after which it showed a decrease.

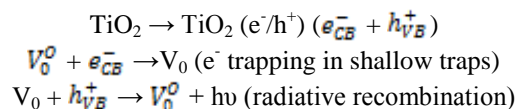
A decrease in refractive index was observed with increase in oxygen content in the sputtering chamber. As discussed earlier (section 3.1), sputtering yield decreases as amount of oxygen in the sputtering chamber is increased. Also, since the substrates are maintained at room temperature, diffusivity of the deposited ions decreases. Lower surface mobility is associated with a porous and void rich structure, which results in lower packing density of the films, and hence refractive index decreases [55]. Similar reports of declining refractive index with increase in oxygen partial pressure in case of dc magnetron sputtered titanium dioxide and tantalum oxide films has been reported by S. B. Amor et al and T. M. Ngaruiya et al, respectively [57, 58]. Extinction coefficient also decreases with increase in oxygen content in the sputtering chamber. At low oxygen pressures, the films contain a large number of oxygen vacancies, which results in enhancement of absorption coefficient and hence an increase in extinction coefficient. As oxygen content increases, the oxygen vacancies are filled up, resulting in decrease of extinction coefficient.

As can be seen from Table 1, an increase in optical band gap was accompanied by a decrease in refractive index. This trend is consistent with the 'Moss rule' connecting optical band gap and refractive index [59]. This observation has been confirmed by various authors [60, 61, 62]

3.5 Photoluminescence studies

Photoluminescence spectra of TiO₂ thin films, deposited at various substrate temperatures and Ar:O₂ ratios, and excited using light of wavelength 320nm is shown in Figs. 9 and 11 respectively. PL spectra are featured by two prominent emissions: (a) in the UV region and (b) a defect-related deep level emission in the visible region. UV emission peak is associated with exciton

recombination. Visible luminescence is mainly due to structural defects and surface defects. Structural defects are usually related to deep level emissions like oxygen vacancies. The reduced TiO₂ surface (oxygen vacancy) is of particular interest for its photocatalysis applications such as dehydration of formic acid and dissociation of water molecules [63, 64]. Electron trap states caused by oxygen vacancies are located 0.5-1 eV below the bottom of conduction band for TiO₂ materials [65, 66]. The presence of oxygen vacancy levels located 0.23 – 1.29 eV below the conduction band in dc sputtered TiO₂ thin films deposited at various oxygen partial pressures has been reported by Z.Qing-nan et al [67]. Defects and vacancies in semiconductors can lead to the formation of localized states near the conduction band edge. Emissions from these states lead to luminescence in the visible region. Ghosh et al [68] has detected several defect energy levels. The defect energy levels can be understood from the following relations [69]:



where V_0^O in the Kroger notation is an ionized oxygen vacancy level which rapidly traps a photogenerated CB electron e_{CB}^- which subsequently interacts with a VB hole h_{VB}^+ either radiatively or non-radiatively.

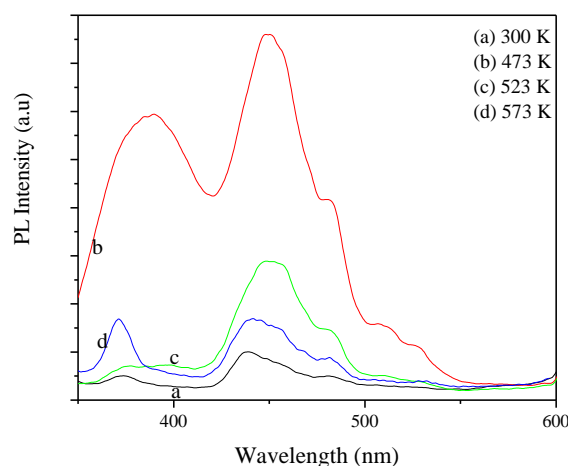


Fig. 9. Photoluminescence spectra of TiO₂ thin films deposited at various substrate temperatures (300 W, 0.01mbar) and post annealed at 873 K.

For the films deposited at various substrate temperatures, UV emission is observed at 371.23 nm for the samples ST1 and ST4 and at 385.17 nm for the sample ST2. This emission can be attributed to excitons trapped at shallow level defects. Self-trapping theory by Toyozawa [70] suggests that two competing processes follow excitation. One is the localization process where the excited state induces a local distortion. The other is the delocalization process in which the excited state lowers its

energy by transferring from one site to neighboring site, forming an exciton band. They have reported that excitons in anatase are in self trapped state, which is characterized by strong electron-phonon coupling and small exciton band width. It is also well known that for small semiconductor particles, non-radiative transitions will be dominant if there is strong coupling of wave functions of trapped electrons and trapped holes. Non-radiative transitions to shallow level defects, followed by the recombination of trapped excitons in these levels contribute to the emission observed in the UV region. FWHM of the UV emission peak is least for the sample ST4, which denotes better crystallinity of the sample. This is evident in the XRD images also, which shows three significant peaks corresponding to anatase phase.

Emissions in the blue region observed at 436.56 nm for the samples ST1 and ST4 and at 449.98 nm for the samples ST2, ST3 and ST4. This emission is associated with electron transitions from the shallow level of oxygen

vacancies to the valance band. Indirect recombination via defects accounts for the visible emission at 481 nm observed in all the samples [31]. P. M. Kumar et al has attributed the peak at 2.59 eV to electron transitions from levels of Ti⁴⁺ ions adjacent to oxygen vacancies (intragap surface states) [71]. In addition, weak shoulder peaks was observed at 508.89 and 527.67 nm (green emission) for the sample ST2. Peaks in blue and green region are observed for the sample ST2 indicating that there are more oxygen vacancies in the sample. The presence of oxygen vacancies in RF magnetron sputtered TiO₂ thin films has been reported in our previous work using XPS analysis [37]. Intensity of the UV and blue emissions is also very high for the sample ST2, which shows an amorphous nature when analyzed using XRD. A schematic diagram for PL transitions for a representative sample ST2 is shown in Fig. 10.

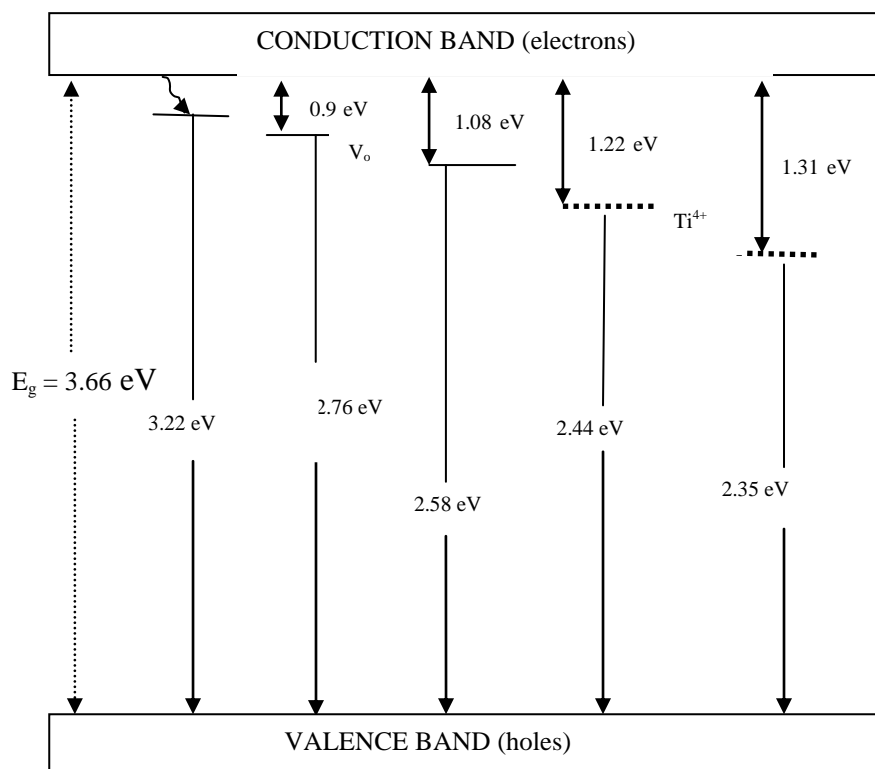


Fig. 10. Schematic representation of PL emission in TiO₂ thin film deposited at 473 K, 300W, 0.01 mbar and thermally annealed at 873 K.

PL spectrum is highly dependent on the amount of oxygen in the chamber during sputtering. Peak at 375 nm observed in all the samples may be attributed to excitons trapped at shallow levels close to the band edges. The intensity of this peak is maximum for the film AO1. Emission from the oxygen vacancy level to the valance band results in the visible emission (blue) at 445 nm for the film AO1. For the film AO2, this emission is absent due to better stoichiometry of films (decrease in defects)

with increase in oxygen content. But a visible emission at 434 nm is observed in the film AO3. When more oxygen is introduced into the chamber, new defect levels are created by the presence of excess oxygen. Transitions from these newly created defect levels accounts for the blue emission in the sample AO3. The weak emission peak at 482 nm for the samples AO1 and AO3 is associated with the indirect recombination via defect states in TiO₂ lattice [72].

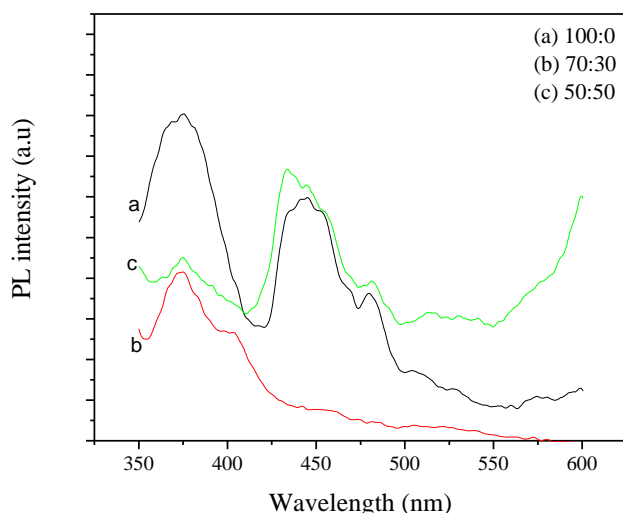


Fig. 11. PL spectra of TiO_2 thin films deposited at various Ar- O_2 ratios (300 W, 0.01 mbar) and post annealed at 873 K.

PL studies show that variations in substrate temperature and Ar: O_2 ratio can be effectively utilized to tune the optical properties of TiO_2 thin films for application in various optoelectronic devices and as light emitters in the visible region. Since RF magnetron sputtering can produce large area coatings these films are suitable for industrial applications such as in display devices.

4. Conclusion

TiO_2 thin films were deposited at different substrate temperatures and Ar: O_2 ratios by RF magnetron sputtering. X-ray analysis of the films prepared at lower substrate temperature revealed the evolution of amorphous-like TiO_2 films, even after post-deposition annealing at 873 K. XRD peaks within detectable limits corresponding to anatase phase was observed only in the film deposited at substrate temperature 573 K, and post annealed at 873 K. The lower surface mobility of the deposited ions might be the reason for the amorphous-like nature of the films when deposited at lower substrate temperatures. However, micro Raman analysis confirmed the presence of short range order in the samples and the formation of anatase and rutile phases. Increase in oxygen content (50:50) has resulted in the formation of amorphous films. This has been confirmed by both XRD and micro Raman analysis. Surface morphologies of the films are highly dependent on the substrate temperature and Ar: O_2 ratio, which is clearly evident from the SEM and AFM images. The variation of Ar: O_2 ratio offers better tunability of band gap than the variations in substrate temperature. The larger value of optical band gap in the sputtered films compared to that of the bulk is explained in terms of quantum size effect that is observed in semiconductors of small particle sizes. PL emission in the UV (excitonic emission) and visible

(defect level emission) regions were observed in the prepared samples which suggests the application of these films in various display devices. But defect related visible emissions were absent in the film prepared in the Ar: O_2 ratio 70:30.

Acknowledgement

One of the authors (P.V.T) wishes to thank the University Grants Commission, New Delhi for the financial assistance (F.No.39-503/2010(SR)).

References

- [1] A. Fujishima, K. Honda, *Nature*, **238** 37 (1972).
- [2] R. Hoffmann, T. Martin, Y. Choi, W. Bahnemann, *Chem. Rev.* **95**, 69 (1995).
- [3] J. Robertson, P. Robertson, L. Lawto, *J. Photochem. Photobiol. A Chem.* **175**, 51 (2005).
- [4] J. Carey, J. Lawrence, H. Tesnie, *Bull. Environ. Contam. Toxicol.* **16**, 697 (1976).
- [5] V. Nadochenko, A. Rincon, S. Stanca, J. Kiwi, J. *Photochem. Photobiol. A Chem.* **169**, 131 (2005).
- [6] A. Fujishima, N. R. Tata, A. Tryk, *J. Photochem. Photobiol. C: Photochem. Rev.* **1**, 1 (2000).
- [7] H. Dislich, P. Hinz, *J. Non. Cryst. Solids* **48**, 11 (1982).
- [8] B. Yoldas, *Appl. Opt.* **19**, 1425 (1980).
- [9] R. W. Phillips, J. W. Dodds, *Appl. Opt.* **20**, 40 (1981).
- [10] J. Livage, *MRS Symp. Proc.* **73**, 717 (1986).
- [11] T. Yoko, K. Kamiya, A. Yuasa, K. Tanaka, S. Sakka, *J. Non. Cryst. Solids* **10**, 483 (1988).
- [12] Y. H. Lee, *Vacuum* **51**, 503 (1998).
- [13] M. Ferrara, *Nanostruct. Mater.* **7**, 709 (1996).
- [14] S. Murugesan, P. Kuppasami, Mohandas, *J. of Nanoscience and Nanoscience*, **9**(9), 5311 (2009).
- [15] B. O. Regan, M. Gratzel, *Nature*, **353**, 737 (1991).
- [16] V. Stranak, C. Martin, M. Quaaas, S. Block, R. Bogdanowicz, S. Kment, H. Wulff, Z. Hubicka, C. A. Helm, M. Tichy, R. Hippler *J. Phys. D: Appl. Phys.* **42**, 105204 (2009).
- [17] E. Halary, E. Haro-Poniatowski, G. Benvenoti, P. Hoffman, *Appl. Surf. Sci.* **168**, 61 (2000).
- [18] A. Amin, D. Kohl, M. Wuttig, *J. Phys. D: Appl. Phys.* **43**, 405303 (2010).
- [19] I. Hotovy, A. Pullmannova, M. Predanocy, J. Hotovy, V. Rehacek, T. Kups, L. Spiess, *J. of Elec. Engg.*, **60**(6), 354 (2009).
- [20] Y. Leprince-Wang, K. Yu-Zhang, *Surf. Coat. Technol.* **140**, 155 (2001).
- [21] D. Lucaa, L. S. Hsu, *J. Optoelectron. Adv. Mater.* **5**(4), 835 (2003).
- [22] M. R. Kozlowski, P. S. Tyler, W. H. Smyrl, R. T. Atanasoski, *J. Electrochem. Soc.* **136**, 442 (1989).
- [23] B. M. Henry, US Patent 4, 200, 474 (1978).
- [24] M. Lottianx, C. Boulesteix, G. Nihoul, F. Varnier, F. Flory, R. Galindo, E. Pelletier, *Thin Solid Films* **170**, 107 (1989).

- [25] D. Mardare, P. Hones, *Mat. Sci. and Engg. B* **68**, 42 (1999).
- [26] Z. C. Jin, I. Hamberg, C. G. Granqvist, *J. Appl. Phys.* **64**, 5117 (1988).
- [27] K. S. Yeung, Y. W. Lam, *Thin Solid Films* **109**, 169 (1983).
- [28] L. M. Williams, D. W. Hess, *J. Vac. Sci. Tech. A*, **1**, 1810 (1983).
- [29] J. Yu, X. Zhao, J. Du, W. Chen, *J. Sol-Gel Sci. Technol.* **17**(2), 163 (2000).
- [30] T. Masahiro, I. Narumi, K. Shigeru, F. Ryoza, *Appl. Surf. Sci.* **169-170**, 535 (2001).
- [31] Q. Ye, P. Y. Liu, Z. F. Tang, L. Zhai, *Vacuum* **81**, 627 (2007).
- [32] N. M. Hasan, A. S. M. A. Haseeb, R. Saidur, H. H. Masjuki, *Int. J. of Che. and Biomolecular Engg.* **1,2**, 93 (2008).
- [33] N. Martin, C. Rousselot, D. Rondot, F. Palmينو, R. Mercier, *Thin solid films* **300** 113 (1997).
- [34] D. Yoo, I. Kim, S. Kim, C. H. Hahn, C. Lee, S. Cho, *Appl. Surf. Sci.* **253**, 3888 (2007).
- [35] S. Dangtip, N. Sripongphan, N. Boonyopakorn, C. Thanachayanont, *Cer. Inter.* **35**, 1281 (2009).
- [36] L. Baoshun, Z. Xiujian, Z. Qingnan, *J. Wuhan Univ. Tech. Mater. Sci. Ed.*, **18**(3), 36.
- [37] Prabitha B. Nair, V. B. Justinictor, G. P. Daniel, K. Joy, V. Ramakrishnan, P. V. Thomas, *Appl. Surf. Sci.* **257**, 10869 (2011).
- [38] R. Swanepoel, *J. Phys. E: Sci. Instrum.* **16**, 1214 (1983).
- [39] M. Sreemany, A. Bose, S. Sen, *Physica B*, **405**, 85 (2010).
- [40] T. Seikiya, S. Ohta, S. Kamei, M. Hanakawa, S. Kurita, *J. Phys. Chem. Solids*, **62**, 717 (2001).
- [41] N. R. Mathews, E. R. Morales, M. A. C. Jacome, J. A. T. Antonio, *Sol. Energy*, **83**, 1499 (2009).
- [42] T. Ohsaka, F. Izumi, Y. Fujiki, *J. Raman Spectrosc.* **7**, 321 (1978).
- [43] Kelly, Sean, Pollak, H. Fred, M. Tomakiewicz, *J. Phys. Chem. B* **101**, 2730 (1997).
- [44] L. Z. Cao, B. L. Cheng, S. Y. Wang, W. Y. Fu, S. Ding, Z. H. Sun, H. T. Yuan, Y. L. Zhou, Z. H. Chen, G. Z. Yang, *J. Phys. D: Appl. Phys.* **39**, 2819 (2006).
- [45] J. A. Thornton, *J. Vac. Sci. Technol.* **11**, 666 (1974).
- [46] T. Takahashi, J. Tanabe, N. Yamada, H. Nakabayashi, *J. Vac. Sci. Technol. A* **4**, 21 (2003).
- [47] Y. R. Park, K. J. Kim, *Thin Solid Films*, **484**, 34 (2005).
- [48] J. Tauc, *Mater. Res. Bull.* **5**(8), 721 (1970).
- [49] R. B. Kale, C. D. Lokhande, *Semicond. Sci. Technol.* **20**, 1 (2005).
- [50] M. Parlak, C. Ercelebi, *Thin Solid Films*, **322**, 334 (1998).
- [51] T. Asanuma, T. Matsutani, C. Liu, T. Mihara, M. J. Kiuchi, *Appl. Phys.* **95**, 6011 (2004).
- [52] N. Martin, C. Rousselot, C. Savall, F. Palmينو, *Thin Solid Films* **287**(1-2), 154 (1996).
- [53] A. L. Linsebigler, G. Q. Lu, J.T. Yates, *Chem. Rev.* **95**, 735 (1995).
- [54] Z. Lide, M. Jimei, *Nanomaterials and Nanostructure*, Science Press, Beijing (2001).
- [55] S. Lin, J. Huang, D. F. Lii, *Surf. and Coat. Tech.* **176**, 173 (2004).
- [56] M. H. Suhail, G. M. Rao, S. Mohan, *J. Appl. Phys.* **71**, 1421 (1992).
- [57] S. B. Amor, G. Baud, J. P. Besse, M. Jacquet, *Thin Solid Films*, **293**, 163 (1997).
- [58] J. M. Ngaruiya, S. Venkataraj, R. Drese, O. Kuppertz, T. P. L. Pedersen, M. Wuttig, *Phys. Status Solidi (A)* **198**, 99 (2004).
- [59] Moss T S *Proc. Phys. Soc. B* **63**, 167 (1950).
- [60] Ghe, L. D. Zhang, G. H. Li, M. Liu, X. J. Wang, *J. Phys. D: Appl. Phys.* **41**, 045304 (2008).
- [61] P. G. Wu, C. H. Ma, J. K. Shang, *Appl. Phys. A* **81**, 1411 (2004).
- [62] S. H. Mohamed, O. Kappertz, J. M. Ngaruiya, T. Niemeier, R. Drese, R. Detemple, M. M. Wakkad, M. Wuttig, *Phys. Status Solidi* **201**, 90 (2004).
- [63] A. Bouzoubaa, A. Markovits, M. Calatayud, C. Minot, *Surface Science* **583**, 107 (2005).
- [64] M. Aizawa, Y. Morikawa, Y. Namai, H. Morikawa, Y. Iwasawa, *J. of Phy. Chem B* **109**, 18831 (2005).
- [65] S. Livraghi, M. C. Paganini, E. Giamello, A. Selloni, C. Di Valentin, G. Pacchioni, *Am. Chem. Soc.* **128**, 15666 (2006).
- [66] M. A. Henderson, W. S. Epling, C. H. F. Peden, C. L. Perkins, *Phys. Chem. B* **107**, 534 (2003).
- [67] Z. Qing-nan, Li Chun-ling, L. Bao-shun, Z. Xiu-jian, *J. Wuhan Univ. Tech.-Mater. Sci. Ed.*, **18**(3), 36 (2003).
- [68] A. K. Ghosh, F. G. Wakim, P. R. Adiss Jr., *Phys. Rev.* **184**, 979 (1969).
- [69] N. Serpone, D. Lawless, R. Khairutdinov, *J. Phys. Chem.* **99**, 16646 (1995).
- [70] Y. Toyozawa, *J. Luminesc.* **12/13**, 13 (1976).
- [71] P. M. Kumar, S. Badrinarayanan, M. Sastry, *Thin Solid Films*, **358**(1-2), 122 (2000).
- [72] B. Liu, X. Zhao, Q. Zhao, X. He, J. Feng, *J. Electron Spectrosc. Relat. Phenom.* **148**, 158 (2005).

*Corresponding author: thomaspv_15@yahoo.com